

# Morphology and Luminescence Regulation for CsPbBr<sub>3</sub> Perovskite Light-Emitting Diodes by Controlling Growth of Low-Dimensional Phases

Zhiqiang Bao, Xiaoyang Guo,\* Kai Sun, Jianfeng Ou, Ying Lv, Deyue Zou, Yantao Li, Li Song,\* and Xingyuan Liu\*



Cite This: *ACS Appl. Mater. Interfaces* 2022, 14, 56374–56383



Read Online

ACCESS |



Metrics & More



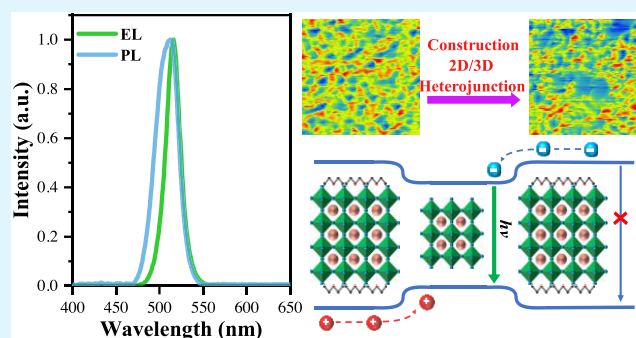
Article Recommendations



Supporting Information

**ABSTRACT:** At present, the high defect density and strong nonradiative recombination rate of all-inorganic cesium lead bromide (CsPbBr<sub>3</sub>) perovskite light-emitting diodes (PeLEDs) seriously inhibit the improvement of their quantum efficiency. In this paper, the addition of a short-chain additive, diethylammonium bromide (DEABr), aims to control the generation of a quasi-2D large n-phase to optimize the surface morphology and construct two-dimensional/three-dimensional (2D/3D) heterojunction perovskite structures to enhance the EL efficiency of PeLEDs. Through Kelvin probe force microscopy (KPFM) characterization, we confirmed that the 2D phase grains with a low potential are locally formed on the surface of the perovskite film under the action of DEABr. The existence of the 2D phase effectively improved the surface morphology and suppressed surface defects. In addition, the in situ constructed 2D/3D heterojunction perovskite structure further increases the exciton radiative recombination rate and significantly improves the electroluminescent performance. By optimizing its doping concentration, the optimal all-inorganic PeLED displays a current efficiency (CE) of 30.3 cd A<sup>-1</sup>, an external quantum efficiency (EQE) of 9.6%, and a maximum brightness of 32,500 cd m<sup>-2</sup>. According to our results, the formation of 2D structures on the surface of the CsPbBr<sub>3</sub> film can improve surface morphology issues and optoelectronic properties of the film.

**KEYWORDS:** perovskite light-emitting diodes, surface morphology, 2D/3D heterojunction, Kelvin probe force microscopy, in situ constructed



## 1. INTRODUCTION

As a popular semiconductor material, lead halide perovskite has attracted great scientific interest in the field of optoelectronics, such as photovoltaic cells (PSCs), light-emitting diodes (LEDs), lasers, and detectors.<sup>1–6</sup> In particular, the excellent optical and electrical properties, such as high photoluminescence quantum efficiency (PLQY), tunable band gap, high carrier mobility, and high color purity, as well as its solution processability, have broad application prospects in cost-effective and high-performance optoelectronic devices.<sup>7,8</sup> Since the first report in 2014,<sup>9</sup> the use of perovskites as light-emitting materials for LEDs has received extensive attention from researchers, and perovskite light-emitting diodes (PeLEDs) have become an important field of scientific research. In particular, the external quantum efficiency (EQE) of PeLEDs using organic–inorganic hybrid perovskites and low-dimensional (LD) perovskite structures has exceeded 20%.<sup>10–14</sup> However, when organic cations such as methylammonium (MA<sup>+</sup>) or formamidinium (FA<sup>+</sup>) occupy the A site of the perovskite crystal structure, the perovskite structure is

more sensitive to water, electrical stress, and thermal effects,<sup>15,16</sup> which seriously affect the electroluminescence (EL) performance of the device and hinder the development of PeLEDs in practical applications. Therefore, researchers found that inorganic cesium ions (Cs<sup>+</sup>) can be used to prepare all-inorganic perovskite structures with better stability, namely, CsPbX<sub>3</sub> (X = Cl, Br, and I) and their mixtures.<sup>17</sup> However, the EL efficiency of all-inorganic PeLEDs is affected by the poor film formation quality, mainly due to the large grain size and high defect density,<sup>18</sup> resulting in poor EL performance, but with the advantages of a long working life and high stability.<sup>19,20</sup> Therefore, improving the optoelectronic proper-

**Received:** September 27, 2022

**Accepted:** November 24, 2022

**Published:** December 8, 2022



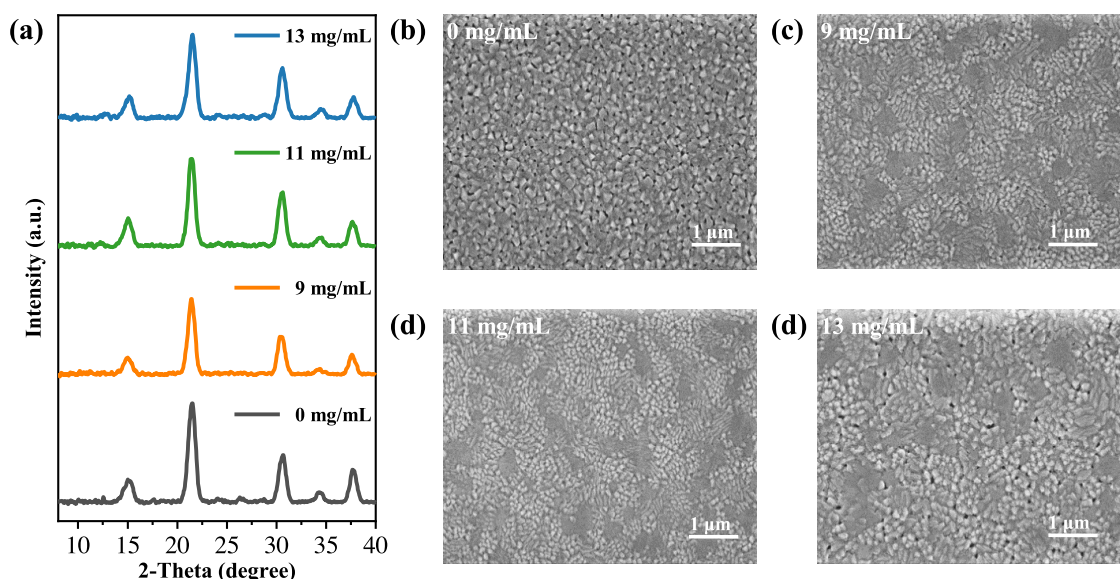


**Figure 1.** (a) XRD patterns of perovskite films fabricated by CsPbBr<sub>3</sub> precursor solutions doped with DEABr (0, 9, 11, and 13 mg/mL). Top-view SEM of the perovskite film with DEABr concentrations of (b) 0 mg/mL, (c) 9 mg/mL, (d) 11 mg/mL, and (e) 13 mg/mL.

ties of all-inorganic PeLEDs may be helpful to realize the commercial application of highly efficient and stable PeLEDs.

Currently, various strategies, such as antisolvent treatment, addition of passivators, composition optimization, and interface-induced crystal growth, have been proposed to address the problems of large grains and high defect density on the surface of the CsPbBr<sub>3</sub> film. In addition to the above strategies, the construction of LD/3D heterophased perovskite structures in the film has been shown to be an effective scheme to achieve stable and efficient PSCs and PeLEDs.<sup>21–23</sup> Adding alkali metal halides such as KBr and CsBr to the precursor solution of CsPbBr<sub>3</sub> can effectively generate the 0D phase structure in the film.<sup>24,25</sup> The deep energy level of the 0D phase effectively confined excitons, which promotes the radiative recombination of the 3D phase and improves the PeLED device efficiency. In addition, adding long-chain organic spacer cations (e.g., phenylethylammonium (PEA<sup>+</sup>) and *n*-butylammonium (BA<sup>+</sup>)) to the precursor solution can generate quasi-2D perovskite structures.<sup>26–29</sup> The quasi-2D phase is more suitable for constructing high-efficiency PeLEDs with two-dimensional/three-dimensional (2D/3D) heterophased structures due to its excellent energy-level arrangement and unique energy cascade transfer channels.<sup>30–32</sup> The quasi-2D phase can significantly improve the EQE of the device, but it will also lead to the problem of nonuniform phase distribution in the film. The presence of the *n* = 1 phase dominated by the nonradiative recombination process will seriously affect the EL performance of the device, while the presence of the large *n*-phase will lead to the broadening of the spectrum and the existence of shoulder emission, so it is necessary to reasonably adjust the distribution of quasi-2D phases in the perovskite film. It has been demonstrated that the 2D/3D heterojunction perovskite structure can avoid the problem of low-dimensional phase distribution to some extent.<sup>33,34</sup> However, there is a lack of research on the heterophased structure constructed from the quasi-2D large *n*-phase and the 3D phase. Especially when no distinct characteristic quasi-2D small *n*-phase is observed, it becomes difficult to prove the existence of the quasi-2D large

*n*-phase close to the 3D grain size and similar optical properties.

In this work, we propose a novel short-chain additive, diethylammonium bromide (DEABr). A quasi-2D large *n*-phase is formed in the perovskite film through the reduced-dimension effect of DEABr, and grain size reduction and close arrangement are induced, resulting in a dense and pinhole-free mixed-phase perovskite film. It was found by Kelvin probe force microscopy (KPFM) characterization that the 2D phase with low potential on the surface of the film will reduce the proportion of grain boundary distribution in the film, which will help reduce the defect density in the film and suppress nonradiative recombination. In addition, a 2D/3D heterojunction structure is constructed between these 2D phases and 3D phases, which will effectively avoid the problems of spectrum broadening and multi-peaks, and the charge carriers are constrained in the 3D structure, thus greatly improving the EQE of the device. Consequently, we fabricated a green PeLED with a current efficiency (CE) of 30.3 cd A<sup>-1</sup> and an external quantum efficiency (EQE) of 9.6% with the brightness of 32,500 cd m<sup>-2</sup>. Our results reveal that controlling the formation of the 2D phase in the 3D perovskite is helpful to improving the film morphology and luminescent properties, and the construction of a 2D/3D heterojunction perovskite provides a feasible development direction for the realization of efficient and stable inorganic PeLEDs.

## 2. EXPERIMENTAL SECTION

**2.1. Materials.** DEABr, PEDOT:PSS (Clevios Al 4083), and TPBi were purchased from Xi'an Polymer Light Technology Corp. Lead bromide (PbBr<sub>2</sub>) was purchased from Liaoning Preferred New Energy Technology Company, and cesium bromide (CsBr) was purchased from Kanto Chemical Co. Ltd. Ethanolamine (EA) was purchased from Sigma-Aldrich. All materials were used directly without further purification.

**2.2. Preparation of Perovskite Precursor Solution.** The CsPbBr<sub>3</sub> precursor solution was prepared by simultaneously dissolving CsBr (65 mg/mL), PbBr<sub>2</sub> (80 mg/mL), and DEABr (0, 9, 11, and 13 mg/mL) in DMSO and stirred at 40 °C for 12 h. In this experiment, perovskite films were prepared by the spin-coating

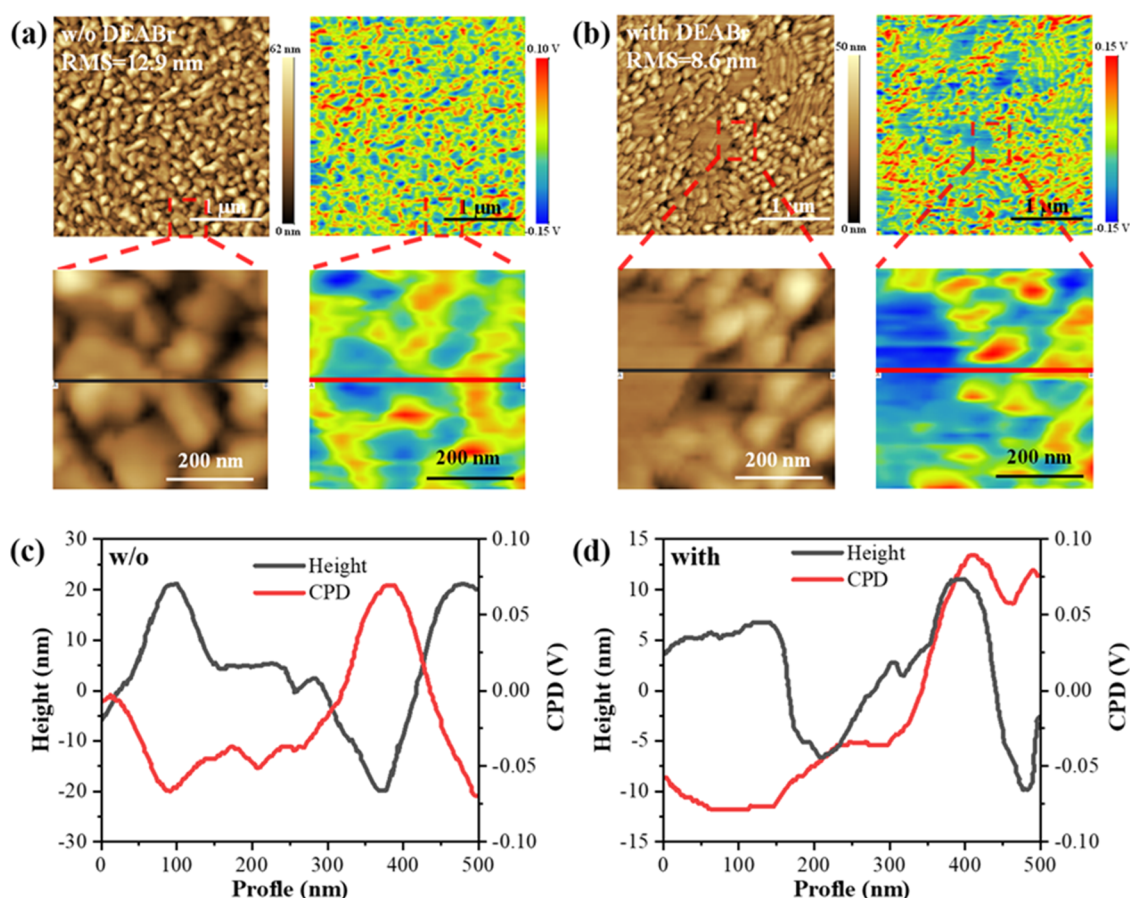


**Figure 2.** Morphology and CPD analysis of suspecting 2D phase grains (a) without and (b) with the DEABr-doped film. Corresponding line profiles extracted from magnified images of (c) topography and (d) CPD.

method, in a glovebox filled with nitrogen, and 100  $\mu\text{L}$  of CsPbBr<sub>3</sub> precursor solutions were dropped on the center of the substrate.

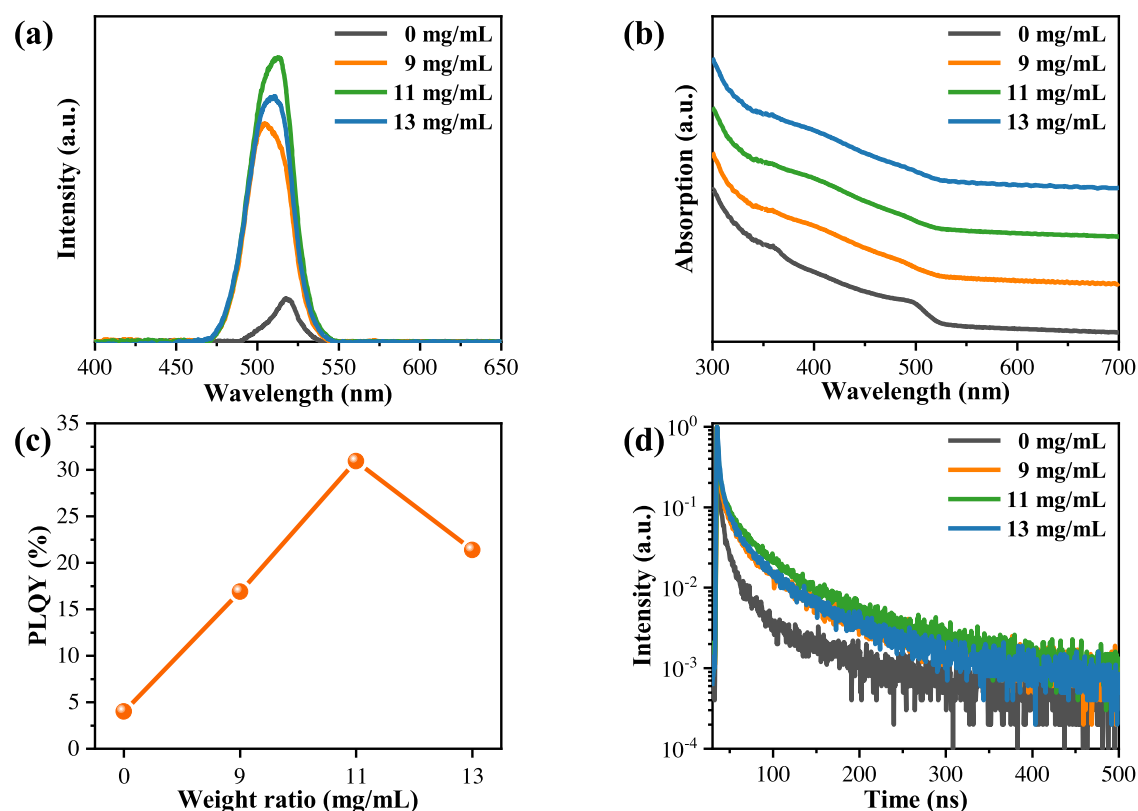
**2.3. Fabrication of PeLEDs.** The ITO electrode before use was cleaned ultrasonically with acetone, ethanol, and deionized water for 20 min each time and then treated in an ultraviolet ozone environment for 30 min. EA was dissolved in ethanol at a volume ratio of 4:20 and added into 1 mL of PEDOT:PSS to produce EA-PEDOT:PSS, and the content of EA was kept at 0.4 vol %.<sup>35,36</sup> The solution of EA-PEDOT:PSS before use was filtered with 0.22  $\mu\text{m}$  of a water-based filter head to remove large particles and insoluble substances. In ambient air, modified EA-PEDOT:PSS was dropped onto the ITO electrode treated with UV ozone, and HTL was prepared by rotating coating at a speed of 2500 rpm for 40 s. The substrate was then placed on a 140  $^{\circ}\text{C}$  hot stage for 15 min. Then, the substrates were transferred to a glovebox filled with nitrogen to prepare perovskite films. The perovskite films were obtained by spin-coating at 4500 rpm for 60 s. Then, the samples were heated at 70  $^{\circ}\text{C}$  for 10 min to improve the crystallization. TPBi (40 nm), LiF (1 nm), and Al (100 nm) were successively evaporated in a piece of thermal evaporation equipment with a vacuum of  $1.0 \times 10^{-4}$  Pa. Evaporation rates were 1, 0.1, and 5  $\text{\AA}/\text{s}$ , respectively. The effective area of PeLED was determined to be 0.08  $\text{cm}^2$  with an overlap between ITO and Al electrodes.

**2.4. Characterization.** The morphology of the CsPbBr<sub>3</sub> film was characterized by SEM (Hitachi 4800). The contact potential difference was analyzed by KPFM with a Shimadzu SPA-9700. The absorption spectra of CsPbBr<sub>3</sub> films were measured by a Shimadzu UV-3101PC. The PL spectra of CsPbBr<sub>3</sub> films were measured by a Hitachi F-7000 fluorescence spectrometer. Time-resolved PL spectra of CsPbBr<sub>3</sub> films were measured by an Edinburgh FLS920 spectrometer. The XRD patterns of perovskite films were measured by a Rigaku SmartLab. The current density–voltage curve and the

luminance–voltage curve of the device were measured using a Keithley 2611 digital source meter and a luminance meter (Konica-Minolta LS-110). The EL spectrum of the device was measured by an optical fiber spectrometer. EQE was calculated based on the brightness, current, and emission spectrum of the hypothetical Lambert emission. All tests were carried out in air and without encapsulation.

### 3. RESULTS AND DISCUSSION

CsPbBr<sub>3</sub> films with various concentrations of DEABr (0, 9, 11, and 13 mg/mL) were fabricated by one-step spin-coating on EA-PEDOT:PSS, and crystal structural analysis was performed by X-ray diffraction (XRD), as illustrated in Figure 1a. The diffraction peaks at 15.2, 21.5, 30.7, 34.3, and 37.7 $^{\circ}$  can be assigned to the (100), (110), (200), (201), and (211) planes of the orthorhombic (*Pnma*) CsPbBr<sub>3</sub> crystal, consistent with previous reports.<sup>37,38</sup> According to the information on the peak positions and intensity ratios of each diffraction peak in the comparison chart, it is found that all perovskite films show almost the same XRD patterns, indicating that the crystal structure and growth orientation of CsPbBr<sub>3</sub> are not significantly affected by the added DEABr. To further investigate the effect of DEABr on the surface morphology of the perovskite film, surface morphologies of DEABr-CsPbBr<sub>3</sub> films with different concentrations were compared by overhead scanning electron microscopy (SEM). In Figure 1b, without DEABr doping (0 mg/mL), the surface of the CsPbBr<sub>3</sub> film is distributed with loose large grains and a large number of pinholes, and the film coverage is poor. As shown in



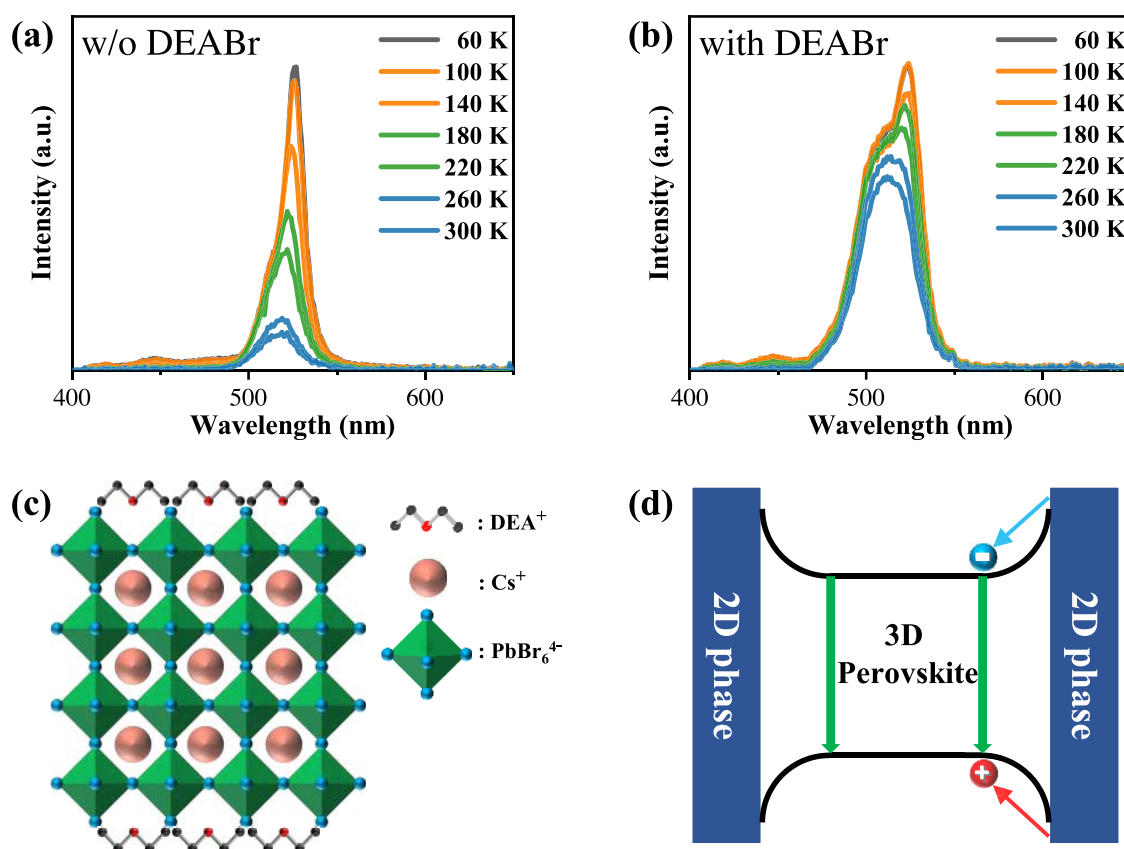
**Figure 3.** Photophysical properties of the DEABr-CsPbBr<sub>3</sub> thin film. (a) PL, (b) absorption spectra, (c) PLQY value changes, and (d) TRPL decay curves of the DEABr-CsPbBr<sub>3</sub> perovskite film with various concentrations.

Figure 1c–e, as the concentration of DEABr was changed to 9, 11, and 13 mg/mL, the film surface randomly grew multiple flat shaded areas. After DEABr doping, we believe that two distinct perovskite phases grew on the surface of the perovskite film, a flat low-dimensional (LD) phase and a small-grained 3D phase (Figure S1). The LD phase of the film may be due to the formation of a quasi-2D perovskite structure dominated by the large n-phase under the hydrogen bonding of DEABr. Since the grain size of the quasi-2D large n-phase perovskite is very close to that of the 3D phase, the diffraction angles in XRD do not change significantly. Second, the formation of the quasi-2D phase may also reduce the crystallization rate and promote the growth of small-grained perovskites, forming a mixed-phase perovskite film dominated by small grains. The formation of the 2D phase suppresses the surface pinholes on the pristine perovskite film, resulting in a dense and pinhole-free CsPbBr<sub>3</sub> film. When the concentration was increased to 13 mg/mL, the pinholes on the surface increased again and the membrane surface coverage decreased. Furthermore, in the statistical histogram of grain size (Figure S2), when DEABr in the film was adjusted from 0 to 9 and 11 mg/mL, the average crystal size of CsPbBr<sub>3</sub> dramatically decreased from 149 to 90 nm and to 79 nm, respectively. However, when the doping amount was adjusted to 13 mg/mL, the average crystal size increased to 107 nm, which indicates that excessive DEABr increases the formation of large grains and deteriorates the surface morphology of the perovskite films.

To further understand the mixed distribution of different crystalline phases on the surface of the perovskite film, Kelvin probe force microscopy (KPFM) characterization was performed. The surface topography and contact potential difference (CPD) spatial maps of the DEABr-CsPbBr<sub>3</sub> samples

were measured, as shown in Figure 2a,b. In Figure 2b, similar features to those in the SEM image can be observed, with some relatively large and flat 2D phase grains randomly distributed over the entire film surface. As a result, the root-mean-square (RMS) roughness of the perovskite film decreases from 12.9 to 8.6 nm. Subsequently, in the local amplification images, grains with the same characteristics were selected for the morphology and CPD profile, and the corresponding line profiles are illustrated in Figure 2c,d. We can find that the topography and CPD profiles are dissimilar, which ensures that the topographic features are not correlated with the CPD measurements.<sup>39–41</sup>

In Figure 2c, it can be found that the CPD of the crystal grains (blue region) in the undoped CsPbBr<sub>3</sub> film is smaller than that at the grain boundary (yellow and red regions), and the difference between the two is about 0.1–0.125 V. In Figure 2d, in the CsPbBr<sub>3</sub> sample doped with DEABr, the CPD difference between flat grains and small grains is about 0.05 V, and the CPD difference between small grains and grain boundaries is also 0.1–0.125 V. The CPD map directly reflects the distribution of the work function difference, and it is obvious that the main grains in the two films are 3D phase grains, while the randomly distributed flat grains are 2D phase grains. This proves that the DEABr-CsPbBr<sub>3</sub> is a perovskite film with mixed phase distribution. By comparing the KPFM images of CsPbBr<sub>3</sub> samples doped with/without DEABr, it can be noted that the grain distribution with a low work function increases on the surface of the film, while the grain boundary distribution of a high work function decreases. This phenomenon indicates that DEABr plays an active role in the passivation of grain boundaries in the perovskite film. During the film formation, additives hindered the growth of large grains and formed a perovskite film with a mixed



**Figure 4.** Temperature-dependent characteristics of the DEABr-CsPbBr<sub>3</sub> film. Temperature-dependent PL spectra of the perovskite film (a) without and (b) with DEABr. (c) Schematic diagram of the quasi-2D perovskite structure based on DEABr. (d) Band alignment of the 2D/3D heterojunction perovskite structure.

distribution of small grains and flat grains. In conclusion, doping the DEABr additive will help in the fabrication of smaller-sized grains and a smoother film surface morphology, which is beneficial to the charge transport and radiative recombination of perovskite, which plays a crucial role in realizing high-efficiency PeLEDs.

In Figure 3a, the relative PL intensity of the film enhances greatly with the increase of the DEABr concentration, and the luminescence intensity is the highest when the content is 11 mg/mL. Obviously, the PL of the perovskite film shows a wide full width at half-maximum (FWHM) and asymmetry. The existence may be the luminescence phenomenon of two luminescence peaks' coexistence. We differentiated the PL spectra of the film by the Gaussian fitting, yielding Gaussian peaks at approximately 499 and 515 nm, where the fitting root mean square  $R^2 > 0.998$  (Figure S3). At the same time, based on the Gaussian fitting results, the excitation emission spectra of the two peaks are tested. The test results show that the two luminescence peaks come from two different perovskite phases, which are consistent with the above analysis results. According to previous reports, the coexistence of multiple luminescence peaks in the perovskite film is due to the generation of mixed perovskite phase structures within the film, such as 0D/3D, 2D/3D, and quasi-2D/3D composite perovskite films.<sup>42–45</sup> Due to the uneven distribution of the mixed perovskite phase inside the film, the carriers do not entirely migrate to the perovskites with a small band gap during the energy transfer process,<sup>34,46–48</sup> so the luminescence phenomenon of the coexistence of the LD phase and the 3D phase appears. In Figure 3b, with the increase of DEABr, the absorption peak in

the absorption curve gradually decreases. There is no obvious absorption peak of the LD phase in the absorption curve, that is, the absorption peak of the quasi-two-dimensional small n-phase and the 0D phase. Therefore, we speculate that a quasi-2D large n-phase with similar absorption properties to the 3D phase may be formed, resulting in the weakening of the absorption peak.

To understand the carrier dynamics in the perovskite film, PLQY and TRPL spectra of perovskite films were also investigated. In Figure 3c, the PLQY values of the films with various doping concentrations correspond to 4.01, 16.9, 30.94, and 21.37%. In Figure 3e, the carrier lifetime of the doped film is significantly prolonged and reaches the longest value with the DEABr doping ratio of 11 mg/mL. The average PL lifetimes of DEABr-CsPbBr<sub>3</sub> doped with different concentrations are calculated to be 20.02, 36.77, 38.82, and 29.04 ns (Table S1). To further understand the effect of DEABr on defect suppression, the nonradiative recombination rates of films with different doping concentrations were calculated. The radiative and nonradiative recombination rates can be calculated from the average PL lifetime  $\tau_{\text{avg}}$  and PLQY

$$\tau_{\text{avg}} = \frac{1}{k_r + k_{\text{nr}}} \quad (1)$$

$$\text{PLQY} = \frac{k_r}{k_r + k_{\text{nr}}} \quad (2)$$

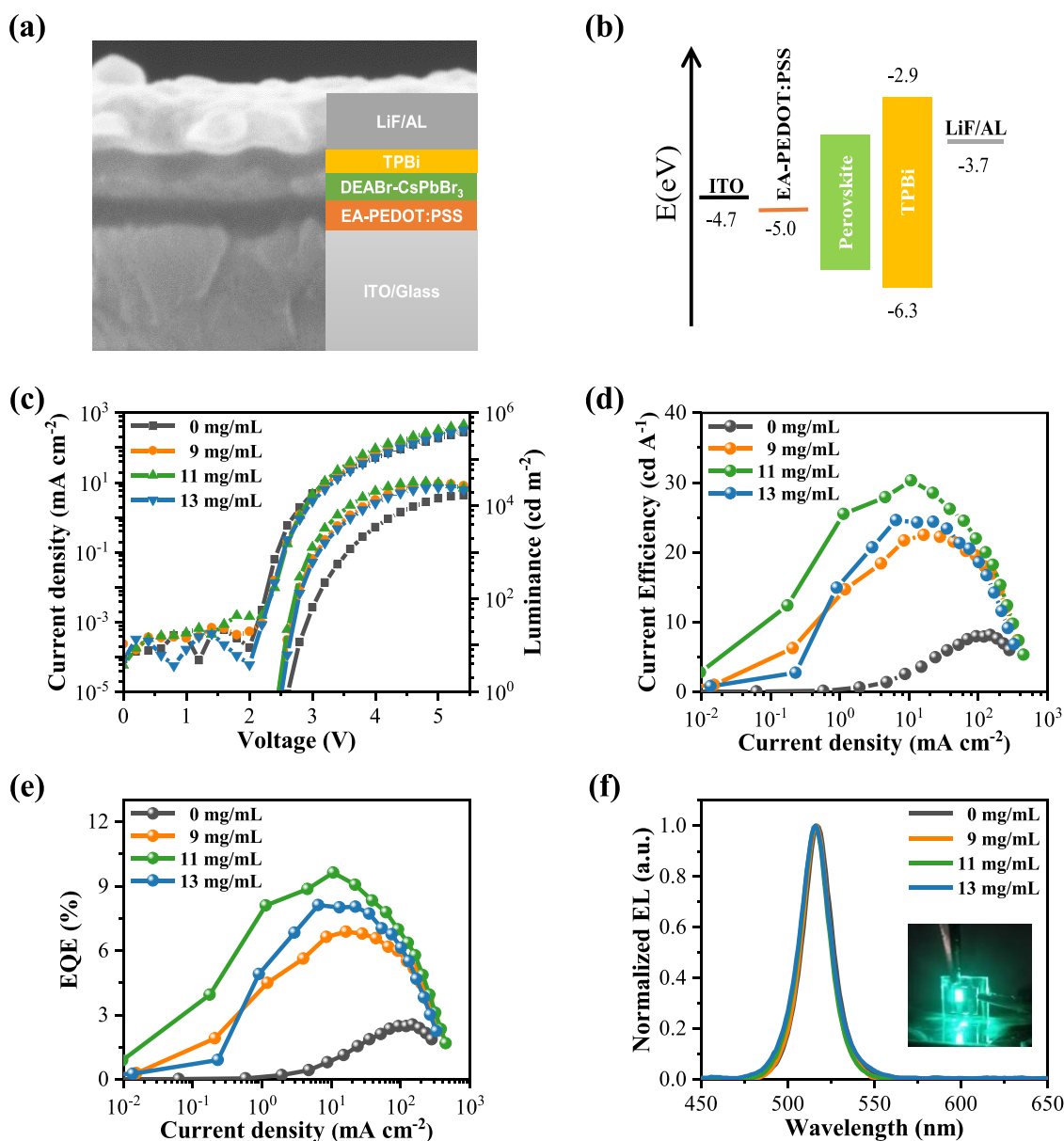


**Figure 5.** (a) Cross-sectional SEM image and schematic diagram of the structure of the DEABr-CsPbBr<sub>3</sub> PeLED. (b) Energy band diagram of the PeLED. (c)  $J$ - $V$ - $L$ , (d)  $CE$ - $J$ , and (e)  $EQE$ - $J$  of the PeLEDs with various doping concentrations of DEABr. (f) EL spectra of devices with various doping concentrations at an operating voltage of 4.0 V. (Inset: a photo of the best PeLED at 4.0 V applied voltage).

where  $k_r$  and  $k_{nr}$  represent radiative and nonradiative recombination rates, respectively. Thus, the nonradiative recombination rate can be deduced as

$$k_{nr} = \frac{1 - PLQY}{\tau_{avg}} \quad (3)$$

It can be seen from the formula that the nonradiative recombination rate of the film is negatively related to PLQY and inversely proportional to  $\tau_{avg}$ . Therefore, films with a higher PLQY and longer average PL lifetimes exhibit lower nonradiative recombination rates. According to the formula calculation, the nonradiative recombination rates of 0, 9, 11, and 13 mg/mL DEABr-CsPbBr<sub>3</sub> films are  $4.79 \times 10^7$ ,  $2.26 \times 10^7$ ,  $1.78 \times 10^7$ , and  $2.71 \times 10^7$  s<sup>-1</sup>, respectively. When the doping concentration is 11 mg/mL, the calculated nonradiative recombination rate is the lowest, indicating that it has the strongest inhibitory effect on nonradiative recombination.

To estimate the trap density in the DEABr-CsPbBr<sub>3</sub> film under different conditions, we fabricated hole-only devices using the device structure of ITO/EA-PEDOT:PSS/perovskite/MoO<sub>3</sub>/Ag (Figure S4). Based on the current density-voltage characteristics of hole-only devices, a space-charge-limited current (SCLC) analysis was performed.<sup>4</sup> Comparing the trap filling limiting voltage ( $V_{TFL}$ ) of DEABr samples with different concentrations, the  $V_{TFL}$  values of 0, 9, 11, and 13 mg/mL were 0.25, 0.23, 0.20, and 0.26 V, respectively. It can be found that when the concentration of DEABr is adjusted to 11 mg/mL, the trap density of the perovskite film reaches the lowest level, and an appropriate amount of DEABr doping can effectively reduce the trap states in the perovskite film, which can be used to prepare efficient and stable PeLEDs. The excellent optical properties of the DEABr-CsPbBr<sub>3</sub> film originate from the formation of small grains and the existence of a mixed-phase perovskite structure, which can effectively

**Table 1. Electrical Output Characteristics of All-Inorganic PeLEDs Doped with Different Concentrations of DEABr**

DEABr (mg/mL)	$V_{on}$ (V)	max. L (cd m <sup>-2</sup> )	CE (cd A <sup>-1</sup> )	EQE (%)	CIE
0	2.62	17,000	8.1	2.6	(0.103,0.745)
9	2.49	30,000	22.5	6.9	(0.075,0.774)
11	2.46	32,500	30.3	9.6	(0.079,0.751)
13	2.51	25,000	24.6	8.1	(0.101,0.717)

generate excitons and sterically confine their diffusion, reduce defect states, and enhance the radiative recombination efficiency of the perovskite film. Through the characterization of optical properties, it is proved that the doping performance of 11 mg/mL DEABr is the optimal concentration, and the fabricated perovskite film gets the best optical performance.

To reveal the excitonic properties in the perovskite film after DEABr doping, we tested the temperature-dependent PL spectra. The temperature-dependent steady-state PL spectra of perovskites of 0 and 11 mg/mL DEABr-CsPbBr<sub>3</sub> are shown in Figure 4a,b. When the temperature is gradually increased from 60 to 300 K, the corresponding PL intensity gradually decreases, which is attributed to the thermal quenching of the PL emission. The perovskites on the EA-PEDOT:PSS substrate both exhibit multiple luminescence peaks, of which the two distinguishable peaks are located at 417 and 447 nm, which correspond to the  $n = 2$  and 3 low-dimensional phases, respectively. This may be the low-dimensional phase luminescence caused by the interaction between EA and the perovskite at the contact interface,<sup>49</sup> but it can be completely quenched when the temperature reaches above 180 K. After the addition of DEABr, the luminescence of the 2D structure was not completely quenched by the increase of temperature but overlapped with the luminescence of the 3D structure to form a broad PL spectrum. Because the luminescence peaks of the 2D and 3D phases are highly overlapping, it is difficult to dissociate them and calculate the exciton binding energy.

It is well known that hydrogen bonding occurs between the ammonium ion (NH<sub>3</sub><sup>+</sup>) in the organic ammonium bromide and the Br<sup>-</sup> on the inorganic octahedra. Therefore, we speculate that controlled size and structural growth of perovskites are related to doped imino units (-NH-).<sup>50,51</sup> According to the literature, the radius of the DEA<sup>+</sup> cation is larger than that of organic A-site cations (such as the ethylammonium ion (EA<sup>+</sup>), dimethylammonium ion (DMA<sup>+</sup>), etc.),<sup>52,53</sup> so we believe that DEA<sup>+</sup> is difficult to dope into 3D perovskite crystals. Considering that the ability of imino groups in DEA<sup>+</sup> to act as hydrogen-bond donors is weaker than that of amine groups,<sup>54</sup> it is difficult to form an obvious low-dimensional phase signal like PEA<sup>+</sup> and BA<sup>+</sup>, but a quasi-2D large n-phase structure close to 3D will be formed. This is consistent with the analysis of the structural and optical properties of the DEABr-CsPbBr<sub>3</sub> film. Figure 4c shows a schematic diagram of the DEABr-based quasi-2D perovskite structure. Doping of DEABr can provide a halogen-rich environment and hydrogen bonding with the halogen to reduce a large number of vacancy traps (uncoordinated lead ions and halogen vacancies) in the perovskite film, thereby improving the optical properties. Second, DEABr effectively restrained the growth of 3D grains while forming a low-dimensional structure, inducing the close arrangement of 2D and 3D grains on the perovskite surface. Through this close arrangement, a 2D/3D heterojunction structure is formed in the perovskite film, which promotes the charge carriers to be confined in the 3D structure by the 2D structure during the

electroluminescence process, as shown in Figure 4d. This 2D/3D heterojunction structure effectively improves the radiative recombination efficiency of injected carriers and solves the spectral broadening and shoulder emission problems caused by the quasi-2D large n-phase.

To further verify the effect of the 2D/3D heterojunction structure on device performance, PeLED devices with a multilayer structure of glass/ITO/EA-PEDOT:PSS/DEABr-CsPbBr<sub>3</sub>/TPBi/LiF/Al were fabricated, and the cross-sectional SEM of the device structure is shown in Figure 5a. The energy-level distribution map corresponding to the multilayer structure of the device is shown in Figure 5b, and the energy-level values are derived from previous reports.<sup>55</sup> In Figure 5c–e, the current density–voltage–luminance ( $J$ – $V$ – $L$ ), current efficiency–current density (CE– $J$ ), and external quantum efficiency–current density (EQE– $J$ ) characteristics of four devices with different doping qualities are shown. Table 1 summarizes the different concentrations' device performance of DEABr. The optimal device is a PeLED doped with an 11 mg/mL DEABr-CsPbBr<sub>3</sub> film. The turn-on voltage, maximum brightness, current efficiency, and EQE of the device are 2.46 V, 32500 cd m<sup>-2</sup>, 30.3 cd A<sup>-1</sup>, and 9.6%, respectively. In Figure 5f, the electroluminescence (EL) spectra of devices with different doping concentrations at the maximum EQE are shown, and the inset is a photo of the device in operation. We can find that the EL spectrum of the CsPbBr<sub>3</sub> device is not significantly changed after doping with DEABr, and the luminescence peak positions and half-peak width of the devices with and without doping are basically the same. Compared with the PL of the corresponding perovskite film, the 2D phase in the film does not directly participate in the electroluminescence process. The 2D/3D heterojunction structure constructed in the perovskite film effectively solves the problem of 2D phase emission, and the EL of PeLED is still a single 3D phase emission. The optimal DEABr-CsPbBr<sub>3</sub> device exhibits excellent electroluminescence stability at different operating voltages and excellent device repeatability (Figure S5). The optimized PeLED emits green light with the International Commission on Illumination (CIE) coordinates of (0.079,0.751). These results indicate that the enhanced luminescence performance of the perovskite is mainly attributed to the optimization of the CsPbBr<sub>3</sub> thin-film morphology and the constructed 2D/3D heterojunction structure. The effect of the low-dimensional phase in the film on defect passivation and carrier confinement significantly improves the radiative recombination efficiency of the 3D phase, thereby enhancing the electroluminescence performance of PeLEDs.

#### 4. CONCLUSIONS

In conclusion, we report a work utilizing quasi-2D large n-phases to construct 2D/3D heterojunction perovskite structures. By adding DEABr to the precursor solution, 2D grains with a low potential can be self-assembled and the growth of small-sized 3D grains can be controlled, which

significantly improves the surface morphology of the film. At the same time, a 2D/3D heterojunction structure is formed in the film, which effectively solves the problems of spectral broadening and multimodal emission by optimizing the energy band arrangement to affect the carrier transport. The current efficiency and EQE of the PeLED fabricated from the DEABr-CsPbBr<sub>3</sub> film were 30.3 cd A<sup>-1</sup> and 9.6%, respectively, which are significantly improved compared to the pure CsPbBr<sub>3</sub>-based device. This work provides a simple and effective strategy to control the 2D/3D mixture morphology and has important guiding significance for further accurate control of 2D/3D structures.

## ■ ASSOCIATED CONTENT

### SI Supporting Information

The Supporting Information is available free of charge at <https://pubs.acs.org/doi/10.1021/acsami.2c17370>.

High-magnification SEM images of 0 and 11 mg/mL, crystal size distribution of CsPbBr<sub>3</sub> with different concentrations, Gaussian fitting peaks of PL spectra doped with various concentrations of DEABr, excitation emission spectra at different peak positions, current density–voltage curves of hole-only devices, space-charge-limited current measurements, EL spectral stability of PeLED at different bias voltages, statistics of device EQE performance, and CIE color coordinates of optimal devices (PDF)

## ■ AUTHOR INFORMATION

### Corresponding Authors

**Xiaoyang Guo** – State Key Laboratory of Luminescence and Applications, Changchun Institute of Optics, Fine Mechanics and Physics, Chinese Academy of Sciences, Changchun 130033, China; [orcid.org/0000-0003-0259-137X](https://orcid.org/0000-0003-0259-137X); Email: [guoxy@ciomp.ac.cn](mailto:guoxy@ciomp.ac.cn)

**Li Song** – Tianjin Key Laboratory of Electronic Materials and Devices, School of Electronics and Information Engineering, Hebei University of Technology, Tianjin 300401, P. R. China; [orcid.org/0000-0002-4781-4023](https://orcid.org/0000-0002-4781-4023); Email: [songli@hebut.edu.cn](mailto:songli@hebut.edu.cn)

**Xingyuan Liu** – State Key Laboratory of Luminescence and Applications, Changchun Institute of Optics, Fine Mechanics and Physics, Chinese Academy of Sciences, Changchun 130033, China; [orcid.org/0000-0002-9681-1646](https://orcid.org/0000-0002-9681-1646); Email: [liuxy@ciomp.ac.cn](mailto:liuxy@ciomp.ac.cn)

### Authors

**Zhiqiang Bao** – State Key Laboratory of Luminescence and Applications, Changchun Institute of Optics, Fine Mechanics and Physics, Chinese Academy of Sciences, Changchun 130033, China; University of Chinese Academy of Sciences, Beijing 100049, China

**Kai Sun** – State Key Laboratory of Luminescence and Applications, Changchun Institute of Optics, Fine Mechanics and Physics, Chinese Academy of Sciences, Changchun 130033, China; University of Chinese Academy of Sciences, Beijing 100049, China

**Jianfeng Ou** – State Key Laboratory of Luminescence and Applications, Changchun Institute of Optics, Fine Mechanics and Physics, Chinese Academy of Sciences, Changchun 130033, China; University of Chinese Academy of Sciences, Beijing 100049, China

**Ying Lv** – State Key Laboratory of Luminescence and Applications, Changchun Institute of Optics, Fine Mechanics and Physics, Chinese Academy of Sciences, Changchun 130033, China; [orcid.org/0000-0003-1649-5258](https://orcid.org/0000-0003-1649-5258)

**Deyue Zou** – State Key Laboratory of Luminescence and Applications, Changchun Institute of Optics, Fine Mechanics and Physics, Chinese Academy of Sciences, Changchun 130033, China; University of Chinese Academy of Sciences, Beijing 100049, China

**Yantao Li** – State Key Laboratory of Luminescence and Applications, Changchun Institute of Optics, Fine Mechanics and Physics, Chinese Academy of Sciences, Changchun 130033, China

Complete contact information is available at:

<https://pubs.acs.org/10.1021/acsami.2c17370>

### Notes

The authors declare no competing financial interest.

## ■ ACKNOWLEDGMENTS

This work was supported by the National Science Foundation of China Nos. 62175235, 61875195, 51973208, 61975256, and 62035013; the Jilin Province Science and Technology Research Project No. 20220201091GX; and the Project supported by the Dawn Talent Training Program of CIOMP.

## ■ REFERENCES

- (1) Grancini, G.; Nazeeruddin, M. K. Dimensional Tailoring of Hybrid Perovskites for Photovoltaics. *Nat. Rev. Mater.* **2019**, *4*, 4–22.
- (2) Chen, Z.; Li, Z.; Hopper, T. R.; Bakulin, A. A.; Yip, H. L. Materials, Photophysics and Device Engineering of Perovskite Light-Emitting Diodes. *Rep. Prog. Phys.* **2021**, *84*, No. 046401.
- (3) Dong, H.; Zhang, C.; Liu, X.; Yao, J.; Zhao, Y. S. Materials Chemistry and Engineering in Metal Halide Perovskite Lasers. *Chem. Soc. Rev.* **2020**, *49*, 951–982.
- (4) Wang, K.; Yang, D.; Wu, C.; Sanghadasa, M.; Priya, S. Recent Progress in Fundamental Understanding of Halide Perovskite Semiconductors. *Prog. Mater. Sci.* **2019**, *106*, No. 100580.
- (5) Liu, X. K.; Xu, W.; Bai, S.; Jin, Y.; Wang, J.; Friend, R. H.; Gao, F. Metal Halide Perovskites for Light-Emitting Diodes. *Nat. Mater.* **2021**, *20*, 10–21.
- (6) Kang, C. H.; Dursun, I.; Liu, G.; Sinatra, L.; Sun, X.; Kong, M.; Pan, J.; Maity, P.; Ooi, E. N.; Ng, T. K.; Mohammed, O. F.; Bakr, O. M.; Ooi, B. S. High-Speed Colour-Converting Photodetector with All-Inorganic CsPbBr<sub>3</sub> Perovskite Nanocrystals for Ultraviolet Light Communication. *Light: Sci. Appl.* **2019**, *8*, No. 94.
- (7) Quan, L. N.; Rand, B. P.; Friend, R. H.; Mhaisalkar, S. G.; Lee, T. W.; Sargent, E. H. Perovskites for Next-Generation Optical Sources. *Chem. Rev.* **2019**, *119*, 7444–7477.
- (8) Stranks, S. D.; Snaith, H. J. Metal-Halide Perovskites for Photovoltaic and Light-Emitting Devices. *Nat. Nanotechnol.* **2015**, *10*, 391–402.
- (9) Tan, Z. K.; Moghaddam, R. S.; Lai, M. L.; Docampo, P.; Higler, R.; Deschler, F.; Price, M.; Sadhanala, A.; Pazos, L. M.; Credgington, D.; Hanusch, F.; Bein, T.; Snaith, H. J.; Friend, R. H. Bright Light-Emitting Diodes Based on Organometal Halide Perovskite. *Nat. Nanotechnol.* **2014**, *9*, 687–692.
- (10) Lin, K.; Xing, J.; Quan, L. N.; de Arquer, F. P. G.; Gong, X.; Lu, J.; Xie, L.; Zhao, W.; Zhang, D.; Yan, C.; Li, W.; Liu, X.; Lu, Y.; Kirman, J.; Sargent, E. H.; Xiong, Q.; Wei, Z. Perovskite Light-Emitting Diodes with External Quantum Efficiency Exceeding 20 percent. *Nature* **2018**, *562*, 245–248.
- (11) Zhao, B.; Bai, S.; Kim, V.; Lamboll, R.; Shivanna, R.; Auras, F.; Richter, J. M.; Yang, L.; Dai, L.; Alsari, M.; She, X. J.; Liang, L.; Zhang, J.; Lilliu, S.; Gao, P.; Snaith, H. J.; Wang, J.; Greenham, N. C.; Friend, R. H.; Di, D. W. High-Efficiency Perovskite-Polymer Bulk

Heterostructure Light-Emitting Diodes. *Nat. Photonics* **2018**, *12*, 783–789.

(12) Chiba, T.; Hayashi, Y.; Ebe, H.; Hoshi, K.; Sato, J.; Sato, S.; Pu, Y. J.; Ohisa, S.; Kido, J. Anion-Exchange Red Perovskite Quantum Dots with Ammonium Iodine Salts for Highly Efficient Light-Emitting Devices. *Nat. Photonics* **2018**, *12*, 681–687.

(13) Xu, W.; Hu, Q.; Bai, S.; Bao, C.; Miao, Y.; Yuan, Z.; Borzda, T.; Barker, A. J.; Tyukalova, E.; Hu, Z.; Kawecki, M.; Wang, H.; Yan, Z. B.; Liu, X.; Shi, X.; Uvdal, K.; Fahlman, M.; Zhang, W.; Duchamp, M.; Liu, J. M.; Petrozza, A.; Wang, J.; Liu, L. M.; Huang, W.; Gao, F. Rational Molecular Passivation for High-Performance Perovskite Light-Emitting Diodes. *Nat. Photonics* **2019**, *13*, 418–424.

(14) Cao, Y.; Wang, N.; Tian, H.; Guo, J.; Wei, Y.; Chen, H.; Miao, Y.; Zou, W.; Pan, K.; He, Y.; Cao, H.; Ke, Y.; Xu, M.; Wang, Y.; Yang, M.; Du, K.; Fu, Z.; Kong, D.; Dai, D.; Jin, Y.; Li, G.; Li, H.; Peng, Q.; Wang, J.; Huang, W. Perovskite Light-Emitting Diodes Based on Spontaneously Formed Submicrometre-Scale Structures. *Nature* **2018**, *562*, 249–253.

(15) Ye, F.; Shan, Q.; Zeng, H.; Choy, W. C. H. Operational and Spectral Stability of Perovskite Light-Emitting Diodes. *ACS Energy Lett.* **2021**, *6*, 3114–3131.

(16) Niu, G.; Guo, X.; Wang, L. Review of Recent Progress in Chemical Stability of Perovskite Solar Cells. *J. Mater. Chem. A* **2015**, *3*, 8970–8980.

(17) Cho, H.; Wolf, C.; Kim, J. S.; Yun, H. J.; Bae, J. S.; Kim, H.; Heo, J. M.; Ahn, S.; Lee, T. W. High-Efficiency Solution-Processed Inorganic Metal Halide Perovskite Light-Emitting Diodes. *Adv. Mater.* **2017**, *29*, No. 1700579.

(18) Wei, Z.; Perumal, A.; Su, R.; Sushant, S.; Xing, J.; Zhang, Q.; Tan, S. T.; Demir, H. V.; Xiong, Q. Solution-Processed Highly Bright and Durable Cesium Lead Halide Perovskite Light-Emitting Diodes. *Nanoscale* **2016**, *8*, 18021–18026.

(19) Zhang, L.; Yuan, F.; Xi, J.; Jiao, B.; Dong, H.; Li, J.; Wu, Z. Suppressing Ion Migration Enables Stable Perovskite Light-Emitting Diodes with All-Inorganic Strategy. *Adv. Funct. Mater.* **2020**, *30*, No. 2001834.

(20) Wang, H.; Zhang, X.; Wu, Q.; Cao, F.; Yang, D.; Shang, Y.; Ning, Z.; Zhang, W.; Zheng, W.; Yan, Y.; Kershaw, S. V.; Zhang, L.; Rogach, A. L.; Yang, X. Trifluoroacetate Induced Small-Grained CsPbBr<sub>3</sub> Perovskite Films Result in Efficient and Stable Light-Emitting Devices. *Nat. Commun.* **2019**, *10*, No. 665.

(21) Zhang, T.; Xie, L.; Chen, L.; Guo, N.; Li, G.; Tian, Z.; Mao, B.; Zhao, Y. In Situ Fabrication of Highly Luminescent Bifunctional Amino Acid Crosslinked 2D/3D NH<sub>3</sub>C<sub>4</sub>H<sub>9</sub>COO(CH<sub>3</sub>NH<sub>3</sub>PbBr<sub>3</sub>)<sub>n</sub> Perovskite Films. *Adv. Funct. Mater.* **2017**, *27*, No. 1603568.

(22) Wang, Z.; Lu, Y.; Xu, Z.; Hu, J.; Chen, Y.; Zhang, C.; Wang, Y.; Guo, F.; Mai, Y. An Embedding 2D/3D Heterostructure Enables High-Performance FA-Alloyed Flexible Perovskite Solar Cells with Efficiency over 20. *Adv. Sci.* **2021**, *8*, No. 2101856.

(23) Fakharruddin, A.; Qiu, W.; Croes, G.; Devižis, A.; Gegevičius, R.; Vakhnin, A.; Rolin, C.; Genoe, J.; Gehlhaar, R.; Kadashchuk, A.; Gulbinas, V.; Heremans, P. Reduced Efficiency Roll-Off and Improved Stability of Mixed 2D/3D Perovskite Light Emitting Diodes by Balancing Charge Injection. *Adv. Funct. Mater.* **2019**, *29*, No. 1904101.

(24) Kanwat, A.; Yantara, N.; Ng, Y. F.; Hooper, T. J. N.; Rana, P. J. S.; Febriansyah, B.; Harikesh, P. C.; Salim, T.; Vashishta, P.; Mhaisalkar, S. G.; Mathews, N. Stabilizing the Electroluminescence of Halide Perovskites with Potassium Passivation. *ACS Energy Lett.* **2020**, *5*, 1804–1813.

(25) Lin, K.; Yan, C.; Sabatini, R. P.; Feng, W.; Lu, J.; Liu, K.; Ma, D.; Shen, Y.; Zhao, Y.; Li, M.; Tian, C.; Xie, L.; Sargent, E. H.; Wei, Z. Dual-Phase Regulation for High-Efficiency Perovskite Light-Emitting Diodes. *Adv. Funct. Mater.* **2022**, *32*, No. 2200350.

(26) Ban, M.; Zou, Y.; Rivett, J. P. H.; Yang, Y.; Thomas, T. H.; Tan, Y.; Song, T.; Gao, X.; Credgington, D.; Deschler, F.; Sirringhaus, H.; Sun, B. Solution-Processed Perovskite Light Emitting Diodes with Efficiency Exceeding 15% Through Additive-Controlled Nanostructure Tailoring. *Nat. Commun.* **2018**, *9*, No. 3892.

(27) Xiao, Z.; Kerner, R. A.; Zhao, L.; Tran, N. L.; Lee, K. M.; Koh, T. W.; Scholes, G. D.; Rand, B. P. Efficient Perovskite Light-Emitting Diodes Featuring Nanometre-Sized Crystallites. *Nat. Photonics* **2017**, *11*, 108–115.

(28) Jin, G.; Liu, T.; Li, Y.; Zhou, J.; Zhang, D.; Pang, P.; Ye, Z.; Xing, Z.; Xing, G.; Chen, J.; Ma, D. Low-Dimensional Phase Suppression and Defect Passivation of Quasi-2D Perovskites for Efficient Electroluminescence and Low-Threshold Amplified Spontaneous Emission. *Nanoscale* **2022**, *14*, 919–929.

(29) Meng, F.; Liu, X.; Chen, Y.; Cai, X.; Li, M.; Shi, T.; Chen, Z.; Chen, D.; Yip, H. L.; Ramanan, C.; Blom, P. W. M.; Su, S. J. Co-Interlayer Engineering toward Efficient Green Quasi-Two-Dimensional Perovskite Light-Emitting Diodes. *Adv. Funct. Mater.* **2020**, *30*, No. 1910167.

(30) Yuan, M.; Quan, L. N.; Comin, R.; Walters, G.; Sabatini, R.; Voznyy, O.; Hoogland, S.; Zhao, Y.; Beauregard, E. M.; Kanjanaboos, P.; Lu, Z.; Kim, D. H.; Sargent, E. H. Perovskite Energy Funnel for Efficient Light-Emitting Diodes. *Nat. Nanotechnol.* **2016**, *11*, 872–877.

(31) Wang, N.; Cheng, L.; Ge, R.; Zhang, S.; Miao, Y.; Zou, W.; Yi, C.; Sun, Y.; Cao, Y.; Yang, R.; Wei, Y.; Guo, Q.; Ke, Y.; Yu, M.; Jin, Y.; Liu, Y.; Ding, Q.; Di, D.; Yang, L.; Xing, G.; Tian, H.; Jin, C. H.; Gao, F.; Friend, R. H.; Wang, J.; Huang, W. Perovskite Light-Emitting Diodes Based on Solution-Processed Self-Organized Multiple Quantum Wells. *Nat. Photonics* **2016**, *10*, 699–704.

(32) Zhang, L.; Sun, C.; He, T.; Jiang, Y.; Wei, J.; Huang, Y.; Yuan, M. High-Performance Quasi-2D Perovskite Light-Emitting Diodes: From Materials to Devices. *Light: Sci. Appl.* **2021**, *10*, No. 61.

(33) Jiang, N.; Wang, Z.; Zheng, Y.; Guo, Q.; Niu, W.; Zhang, R.; Huang, F.; Chen, D. 2D/3D Heterojunction Perovskite Light-Emitting Diodes with Tunable Ultrapure Blue Emissions. *Nano Energy* **2022**, *97*, No. 107181.

(34) Zhang, F. J.; Cai, B.; Song, J. Z.; Han, B. N.; Zhang, B. S.; Zeng, H. B. Efficient Blue Perovskite Light-Emitting Diodes Boosted by 2D/3D Energy Cascade Channels. *Adv. Funct. Mater.* **2020**, *30*, No. 2001732.

(35) Ou, J.; Guo, X.; Song, L.; Lin, J.; Lv, Y.; Fan, Y.; Li, Y.; Zou, D.; Bao, Z.; Liu, X. Ampholytic Interface Induced in Situ Growth of CsPbBr<sub>3</sub> for Highly Efficient Perovskite Light-Emitting Diodes. *J. Mater. Chem. C* **2021**, *9*, 1025–1033.

(36) Shen, Y.; Li, M. N.; Li, Y.; Xie, F. M.; Wu, H. Y.; Zhang, G. H.; Chen, L.; Lee, S. T.; Tang, J. X. Rational Interface Engineering for Efficient Flexible Perovskite Light-Emitting Diodes. *ACS Nano* **2020**, *14*, 6107–6116.

(37) Schmidt, I.; Olthof, S.; Xu, H.; Meerholz, K. Phosphine Oxide Additives for High-Brightness Inorganic Perovskite Light-Emitting Diodes. *Adv. Opt. Mater.* **2021**, *10*, No. 2101602.

(38) Ou, J.; Guo, X.; Lv, Y.; Fan, Y.; Li, Y.; Zou, D.; Bao, Z.; Song, L.; Liu, X. Efficient Inorganic Perovskite Light-Emitting Diodes by Inducing Grain Arrangement via a Multifunctional Interface. *ACS Appl. Mater. Interfaces* **2021**, *13*, 60571–60580.

(39) Yao, K.; Li, S.; Liu, Z.; Ying, Y.; Dvořák, P.; Fei, L.; Šikola, T.; Huang, H.; Nordlander, P.; Jen, A. K. Y.; Lei, D. Plasmon-Induced Trap Filling at Grain Boundaries in Perovskite Solar Cells. *Light: Sci. Appl.* **2021**, *10*, No. 219.

(40) Chen, S.; Wen, X.; Yun, J. S.; Huang, S.; Green, M.; Jeon, N. J.; Yang, W. S.; Noh, J. H.; Seo, J.; Seok, S. I.; Ho-Baillie, A. Spatial Distribution of Lead Iodide and Local Passivation on Organo-Lead Halide Perovskite. *ACS Appl. Mater. Interfaces* **2017**, *9*, 6072.

(41) Kim, D.; Ahmadi, M. Elucidating the Spatial Dynamics of Charge Carriers in Quasi-Two-Dimensional Perovskites. *ACS Appl. Mater. Interfaces* **2021**, *13*, 35133–35141.

(42) Song, L.; Huang, L.; Liu, Y.; Hu, Y.; Guo, X.; Chang, Y.; Geng, C.; Xu, S.; Zhang, Z.; Zhang, Y.; Luan, N. Efficient and Stable Blue Perovskite Light-Emitting Devices Based on Inorganic Cs<sub>4</sub>PbBr<sub>6</sub> Spaced Low-Dimensional CsPbBr<sub>3</sub> through Synergistic Control of Amino Alcohols and Polymer Additives. *ACS Appl. Mater. Interfaces* **2021**, *13*, 33199–33208.

(43) Fan, R.; Song, L.; Hu, Y.; Guo, X.; Liu, X.; Wang, L.; Geng, C.; Xu, S.; Zhang, Y.; Zhang, Z.; Luan, N.; Bi, W. Boosting the Efficiency and Stability of Perovskite Light-Emitting Devices by a 3-Amino-1-propanol-Tailored PEDOT:PSS Hole Transport Layer. *ACS Appl. Mater. Interfaces* **2020**, *12*, 43331–43338.

(44) Pellegrino, A. L.; Malandrino, G. Surfactant-Free Synthesis of the Full Inorganic Perovskite CsPbBr<sub>3</sub>: Evolution and Phase Stability of CsPbBr<sub>3</sub> vs CsPb<sub>2</sub>Br<sub>5</sub> and Their Photocatalytic Properties. *ACS Appl. Mater. Interfaces* **2021**, *4*, 9431–9439.

(45) Wu, C.; Wu, T.; Yang, Y.; McLeod, J. A.; Wang, Y.; Zou, Y.; Zhai, T.; Li, J.; Ban, M.; Song, T.; Gao, X.; Duhm, S.; Sirringhaus, H.; Sun, B. Alternative Type Two-Dimensional-Three-Dimensional Lead Halide Perovskite with Inorganic Sodium Ions as a Spacer for High-Performance Light-Emitting Diodes. *ACS Nano* **2019**, *13*, 1645–1654.

(46) Li, Z.; Chen, Z.; Yang, Y.; Xue, Q.; Yip, H. L.; Cao, Y. Modulation of Recombination Zone Position for Quasi-Two-Dimensional Blue Perovskite Light-Emitting Diodes with Efficiency Exceeding 5%. *Nat. Commun.* **2019**, *10*, No. 1027.

(47) Shang, Y.; Li, G.; Liu, W.; Ning, Z. Quasi-2D Inorganic CsPbBr<sub>3</sub> Perovskite for Efficient and Stable Light-Emitting Diodes. *Adv. Funct. Mater.* **2018**, *28*, No. 1801193.

(48) Song, J.; Cui, Q.; Li, J.; Xu, J.; Wang, Y.; Xu, L.; Xue, J.; Dong, Y.; Tian, T.; Sun, H.; Zeng, H. Ultralarge All-Inorganic Perovskite Bulk Single Crystal for High-Performance Visible-Infrared Dual-Modal Photodetectors. *Adv. Opt. Mater.* **2017**, *5*, No. 1700157.

(49) Ho, K. T.; Leung, S. F.; Li, T. Y.; Maity, P.; Cheng, B.; Fu, H. C.; Mohammed, O. F.; He, J. H. Surface Effect on 2D Hybrid Perovskite Crystals: Perovskites Using an Ethanolamine Organic Layer as an Example. *Adv. Mater.* **2018**, *30*, No. 1804372.

(50) Tian, Y.; Qian, X. Y.; Qin, C. C.; Cui, M. H.; Li, Y. Q.; Ye, Y. C.; Wang, J. K.; Wang, W. J.; Tang, J. X. Modulating Low-Dimensional Domains of Self-Assembling Quasi-2D Perovskites for Efficient and Spectra-Stable Blue Light-emitting Diodes. *Chem. Eng. J.* **2021**, *415*, No. 129088.

(51) Xing, S.; Lian, Y.; Lai, R.; Cao, X.; Yu, M.; Zhang, G.; Zhao, B.; Di, D. Tuning Precursor-Amine Interactions for Light-Emitting Lead Bromide Perovskites. *J. Phys. Chem. Lett.* **2022**, *13*, 704–710.

(52) Chu, Z.; Zhao, Y.; Ma, F.; Zhang, C. X.; Deng, H.; Gao, F.; Ye, Q.; Meng, J.; Yin, Z.; Zhang, X.; You, J. Large Cation Ethylammonium Incorporated Perovskite for Efficient and Spectra Stable Blue Light-Emitting Diodes. *Nat. Commun.* **2020**, *11*, No. 4165.

(53) Jin, S. Can We Find the Perfect A-Cations for Halide Perovskites? *ACS Energy Lett.* **2021**, *6*, 3386–3389.

(54) Zeng, S.; Shi, S.; Wang, S.; Xiao, Y. Mixed-Ligand Engineering of Quasi-2D Perovskites for Efficient Sky-Blue Light-Emitting Diodes. *J. Mater. Chem. C* **2020**, *8*, 1319–1325.

(55) Cai, L.; Liang, D.; Wang, X.; Zang, J.; Bai, G.; Hong, Z.; Zou, Y.; Song, T.; Sun, B. Efficient and Bright Pure-Blue All-Inorganic Perovskite Light-Emitting Diodes from an Ecofriendly Alloy. *J. Phys. Chem. Lett.* **2021**, *12*, 1747–1753.

## Recommended by ACS

### Interfacial Engineering of Au@Nb<sub>2</sub>CT<sub>x</sub>-MXene Modulates the Growth Strain, Suppresses the Auger Recombination, and Enables an Open-Circuit Voltage of over 1.2 V in Per...

Shuainan Liu, Hongwei Song, *et al.*

JANUARY 13, 2023  
ACS APPLIED MATERIALS & INTERFACES

READ 

### In Situ Observation of Photoinduced Halide Segregation in Mixed Halide Perovskite

Hyunhwa Lee, Jeong Young Park, *et al.*

JANUARY 15, 2023  
ACS APPLIED ENERGY MATERIALS

READ 

### Improvement in Efficiency and Reproducibility for FAPbI<sub>3</sub> Solar Cells with Rapid Crystallization

Qiang Li, Zebo Fang, *et al.*

DECEMBER 25, 2022  
ENERGY & FUELS

READ 

### Versatile Use of 1,12-Diaminododecane as an Efficient Charge Balancer for High-Performance Quantum-Dot Light-Emitting Diodes

Seunghyun Rhee, Jeongkyun Roh, *et al.*

JANUARY 27, 2023  
ACS PHOTONICS

READ 

Get More Suggestions >